Transient Thermal Phenomena and Weld Geometry in GTAW

Thermal cycles and weld geometry can be predicted more accurately with new analytic solutions, infrared vidicon techniques and simple methods for measurement of arc heat transfer described in this paper

BY N. D. MALMUTH, W. F. HALL, B. I. DAVIS AND C. D. ROSEN

ABSTRACT. Three elements that are important in the development of prediction methods for thermal cycles and weld geometry in GTAW are considered in this paper. These are (1) the effect of the latent heat of fusion on a point source simulation, (2) anode heat transfer efficiency for DC straight polarity GTAW and (3) the role of fixture boundary conditions such as those imposed by backing bars. For Item (1), an analytic solution is derived that demonstrates that the molten pool can be considerably elongated at a moderate product of the power and travel speed, due to the energy stored in fusion. In the second item, a new calorimetric concept is studied which gives a relatively simple and inexpensive method of measuring arc efficiency for melting anodes. Finally, in item (3) analytic solutions are developed for predicting the influence of high conductivity backing bars. The predictions are compared with observations using new IR thermographic techniques.

Introduction

Although welding operations occur in almost every conceivable phase of manufacturing, our understanding of the associated physical phenomena needs improvement. Typically, high temperatures and stresses are involved which produce significant alterations of the fabricated material. In practice, quantitative relationships are sought between the process variables, intervening material states, and the desired joint structure. Figure 1 illustrates and amplifies the significance of these relationships for welding processes, some of which have been previously discussed in Ref. 1.

Referring to Fig. 1, items (1) and (2) relate chiefly through the energy input of the arc and the attendant transformations in the workpiece. The vaporized region surrounded by the molten pool interacts strongly with the structure of the arc plasma through electrical and mechanical boundary conditions, which involve surface vapor jets. The unvaporized portion of the pool may be in any of several boiling states. Convection currents will be present in the pool which will affect the temperature distribution in the fused and heat-affected zone and thereby determine phases present and their microstructure, items (2)-(3). For steels, the formation of martensitic structures and the grain size will depend crucially on thermal cycles associated with item (1). Where filler metals are used, the degree of dilution of base metal with filler will also be affected by these thermal cycles, as will residual stresses, porosity and bead cracking.

All of these factors exert a profound influence on weldability, item (5), and the structural integrity of the weldment, item (6). Porosity will be affected by gas solubility and gas entrainment during the heating and cooling process. The mechanical properties of the bead will be strongly influenced by grain size and crystal structure which is controlled according to solidification mechanics primarily by the motion of the phase boundary and the latent heat of fusion.

Finally, the economics, item (7), of the process involve the multiple energy sinks which are associated with radiative, conductive, and convective processes occurring in the electrode, and interactions of the arc with the ambient atmosphere and the workpiece, item (4).

These factors have been particularly apparent in the development of joining processes on the Apollo, B1 and Shuttle, where a recurring set of questions has arisen concerning how acceptance criteria can be met through optimization of fixture design and operating parameters. Judgements based on practical experience have been used to make the necessary tradeoffs between weld quality and strength, to determine the best fixturing to minimize distortion and residual stresses, as well as to determine the power to achieve requisite penetration, among other requirements. The significant cost intrinsic in empirical approaches previously used to attack these problems has motivated an internal research pro-

N. D. MALMUTH is Chairman, Corporate Aerodynamics Panel, W. F. HALL and B. I. DAVIS are associated with Science Center, Rockwell International, Thousand Oaks, California 91360. C. D. ROSEN is affiliated with the Space Division of Rockwell International, Downey, California 90241.

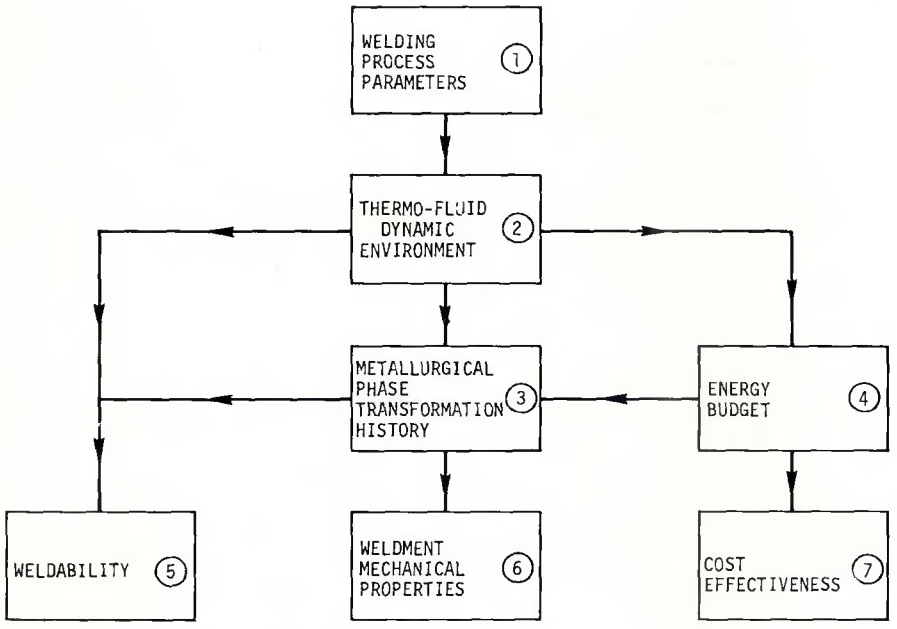

Fig. 1 — Welding input-output relationships

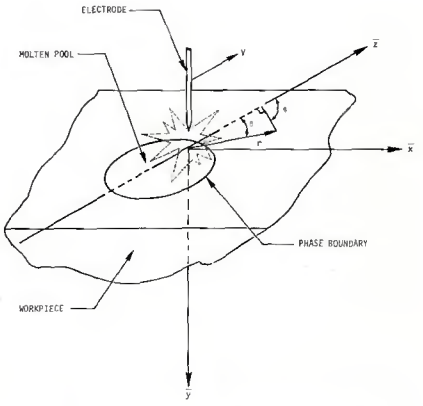

Fig. 2 — Geometry of latent heat problem

gram aimed at understanding on a fundamental level the various interrelationships between GTAW process variables and weld micro and macrostructural formations. This paper will describe new theoretical and experimental developments arising from the study of thermal processes in the workpiece as an element in such relationships.

The focus of the investigation has been the connection among operational parameters, cooling rates, peak temperatures, retention times, and weld geometries. Although the classical Rosenthal moving source theory (Ref. 2) has found application to this area as typified in the analyses of Refs. 3-6, important unknown elements have limited its reliability as a predictive tool. Significant among these is the role of the latent heat of fusion in modifying the molten pool boundary and the associated temperature distribution, the fraction, η, of the arc energy actually reaching the workpiece, i.e., heat transfer efficiency, and finally, the effect of fixture boundary conditions, such as those imposed by backing bars. Our study of these three aspects will be discussed in this paper.

Latent Heat Effects

General Considerations

Within the aims of isolating factors that may affect the temperature distribution in welding, the geometry of the weld pool, the vaporization boundary, and related keyholing phenomena, attention will be given here to the effect of latent heat on the position of a phase change boundary. The reason for selecting this as the initial item of interest is that a simple calculation indicates that in the case of steels, the latent heat can be as high as 30% of the energy required to bring the material to its melting point. The corresponding parameter for vaporization may be ten times higher. Analytical solutions to heat conduction problems of this type are surveyed in Ref. 7, and owing to their nonlinearity, are restricted primarily to one-dimensional systems. Three-dimensional cases appropriate to welding applications have been handled only by numerical methods (Ref. 8) to the authors' knowledge.

To illuminate parametric dependencies, some type of analytic representations of the phase boundary and temperature distributions are required for the three-dimensional situation. Although exact results are unlikely, approximate representations may be obtained using perturbation theory. Such a representation will be developed here for a moving point source simulation of a GTA torch, moving lineally on a workpiece comprising an infinite half space.

Precise limitations on the validity of this approximation for finite thickness workpieces have been given in Refs. 4 and 5. The analysis of Ref. 4 shows that the point source model applies to the thick plate case, in which the thickness, t, of an otherwise infinite workpiece is large compared to a characteristic thermal diffusion length, λ, which is defined as twice the thermal diffusivity, D, divided by the travel speed, V. For "thin" plates, in which $t \ll \lambda$, the line source model is appropriate. The transitional regime when t is of the same order of magnitude as λ will be discussed later in the paper in another connection. It will be noted that analogous methods to those to be now presented can be derived for thin plates.

Formulation of Mathematical Problem

Referring to Fig. 2, the point source is depicted as lying at the origin of the Cartesian set $(\bar{x},\bar{y},\bar{z})$ or the spherical polar set (r,θ,ϕ). The source simulates the welding torch which is stationary in the frame, so that the material moves relative to the torch with the velocity $-V\vec{k}$, where $\vec{k}$ is the unit vector in the $\bar{z}$ direction. The workpiece is assumed to be the infinite half space $\bar{y}>0$. Furthermore, only one phase boundary will be considered for the present, and without loss of generality will be designated as that corresponding to fusion. The case of two boundaries, i.e., vaporization and fusion, will be deferred to another analysis. Denoting $\bar{\rho}$ as the density, κ as conductivity, c = specific heat, D = thermal difusivity $= k/\bar{\rho}c$, L = latent heat of fusion, Q = energy input per unit time of source, and subscripts ℓ and s as representing liquid and solid phases respectively, a boundary value problem for the partial differential equations governing the temperature elevation, T, above ambient conditions (occurring at infinity), can be formulated in terms of the following dimensionless variables

$$\xi_\ell \equiv \frac{Q}{2\pi k_\ell T_m}, \quad \lambda \equiv \frac{2D_\ell}{V}, \quad \alpha \equiv \frac{\xi_\ell}{\lambda}, \quad \kappa \equiv \frac{k_s}{k_\ell}, \quad \delta \equiv \frac{D_s}{D_\ell} \tag{1a}$$

$$\gamma \equiv \frac{L}{cT_m} \tag{1b}$$

$$x \equiv \bar{x}/\lambda, \quad y \equiv \bar{y}/\lambda, \quad z \equiv \bar{z}/\lambda, \quad \rho \equiv \bar{r}/\lambda \tag{1c}$$

$$\tilde{\ell} \equiv T_\ell/T_m, \quad \tilde{s} \equiv T_s/T_m \tag{1d}$$

where it is assumed that the workpiece alloy system changes phase over a narrow enough range of temperatures to be accurately approx-

imated by a single melting temperature, T_m. Furthermore, the change in density upon phase transformation as well as any attendant velocity discontinuity at the phase boundary will be neglected.

Defining

$$\tilde{\sigma} = \tilde{\varsigma}e^{z/\delta}, \quad \tilde{\lambda} = \tilde{\varepsilon}e^{z}$$

$$\Delta = \frac{\partial}{\partial x^2} + \frac{\partial^2}{\partial y^2} + \frac{\partial^2}{\partial z^2} \equiv \frac{1}{r^2}\frac{\partial}{\partial r}\left(r^2\frac{\partial}{\partial r}\right) + \frac{1}{r^2\sin\theta}\frac{\partial}{\partial\theta}\left(\sin\theta\frac{\partial}{\partial\theta}\right) + \frac{1}{r^2\sin^2\phi}\frac{\partial^2}{\partial\phi^2}$$

and without great loss of accuracy letting $\kappa \Rightarrow \delta = 1$, with the symbol, $\tilde{\tau}$, denoting either branch, $\tilde{\sigma}$, and $\tilde{\lambda}$ of the reduced temperature, the exact boundary value problem is:

$$(\Delta - 1)\tilde{\tau} = 0 \tag{2a}$$

$$\lim_{\rho\to\infty} \rho^2\tilde{\tau}_\rho = -\alpha \tag{2b}$$

$$[\nabla\tilde{\tau}\cdot\vec{n}]_I = 2\gamma\tilde{\tau}_I\vec{k}\cdot\vec{n}\ , \quad [\ ]_I \tag{2c}$$

$$\equiv \lim_{\varepsilon\to 0} (\ )_{\rho_I-\varepsilon} - (\ )_{\rho_I-\varepsilon}$$

$$[\tilde{\tau}]_I = 0 \tag{2d}$$

$$\tilde{\tau}_I = e^{\rho_I\cos\theta} \tag{2e}$$

$$\tilde{\tau}e^{\rho\cos\theta} \to 0 \quad \text{as} \quad \rho\to\infty \tag{2f}$$

where the subscript I denotes the solid-liquid interface, and $\vec{n}$ is the unit normal to this surface.

Small Latent Heat-Arbitrary Power Approximation

For most metals, γ associated with fusion is less than unity. For steels, $\gamma = 0.394$, where average values are used, and a reference temperature of 20 C is assumed. This fact motivates a treatment of a limiting class of temperature fields associated with $\gamma \ll 1$. Under these conditions, the normalized temperature $\tilde{\tau}$ as well as the interfacial position ρ_I can be represented in an approximate fashion as small perturbations on their values corresponding to $\gamma = 0$. Thus, it is assumed that

$$\tilde{\tau} = \tilde{\tau}_o + \gamma\tilde{\tau}_1 + \dots \tag{3a}$$

$$\rho_I = R_o + \gamma R_1 + \dots \tag{3b}$$

where the dots signify other corrections that become more important for larger γ's. For the case at hand, only two terms are required for moderately large γ, since $\tilde{\tau}_1$ and R_1 are $\ll 1$. Discussions of perturbation methods using "asymptotic expansions" such as Eqs. (3) are given in works on applied mathematics such as Ref. 9.

Using the approximate expressions, (3), the nonlinear problem (2) can be reduced to a linear sequence of problems for the $\tilde{\tau}_1$'s. These problems may be solved in a manner discussed more thoroughly in Ref. 10, yielding the following results:

$$\tilde{\tau}_o = \frac{\alpha e^{-\rho}}{\rho} \tag{4a}$$

$$1 = \frac{\alpha e^{-R_o}}{R_o} \tag{4b}$$

$$\tilde{\tau}_{o_I} = e^{R_o\cos\theta} \tag{4c}$$

$$\tilde{\tau}_1(\rho,\theta;\alpha) = -2\int_0^{2\pi} d\phi' \int_0^{\pi} \sin\theta' \times R_o'\frac{e^{-R(\rho)+R_o\cos\theta}}{4\pi R(\rho)}\left\{R_o'\cos\theta' + \frac{dR_o'}{d\theta'}\sin\theta'\right\} d\theta' \tag{4d}$$

where:

$$R(\rho) \equiv |\vec{\rho} - R_o(\theta')\vec{1}_{\rho'}|$$

$$\equiv \left[\rho^2 - 2\rho R_o'\cos\beta + R_o'^2\right]^{1/2}$$

$$R_o \equiv R_o(0;\alpha)$$

$$\cos\beta = \vec{1}_\rho\cdot\vec{1}_{\rho'} = \sin\theta\sin\theta' \times \cos\phi' + \cos\theta\cos\theta'$$

$$R_o' \equiv R_o(\theta';\alpha)$$

The interfacial perturbation, R_I is given by:

$$\frac{R_1}{R_o} = \frac{\tilde{\tau}_{1_I}}{\tilde{\tau}_{o_I}[1+R_o(1+\cos\theta)]} \tag{4e}$$

where $\tilde{\tau}_I \equiv \tilde{\tau}_1(R_o,\theta;\alpha)$. For moderate α, the double integral in (4d) can be readily evaluated by numerical methods. One procedure has been developed by E. R. Cohen in Ref. 11, and has been used to obtain some of the numerical results described subsequently.

For $\alpha \to 0$, the case of small power, Eqs. (4) may be simplified using the fact that $R_o' = \alpha$ to give:

$$\tilde{\tau}_1 = -\frac{2}{3}\tilde{\rho}\cos\theta\ , \qquad \rho \leqslant 1$$

$$= -\frac{2}{3}\tilde{\rho}^{-2}\cos\theta\ , \qquad \rho \geqslant 1$$

and

$$R_1 = -\frac{2}{3}\alpha^2\cos\theta$$

where

$$\tilde{\rho} \equiv \rho/\alpha\ .$$

Discussion of Results

In Fig. 3, the solution of this section is compared with the integral equation solution of Ref. 11. The agreement is excellent over the entire θ interval $[0,\pi]$. It is evident from these results which are typical, that the latent heat of fusion exerts an almost negligible effect on the maximum depth of the melting isotherm, at low power levels. This conclusion is analyzed in Ref. 10. Despite the latent heat of fusion being 30-50% of the heat content of the solid at its melting temperature, the energy absorbed in melting the incoming material in the front of the pool is apparently compensated by that liberated in freezing at its rear, a fact not included in previous estimates by other workers.

It is important to note that general pool shape is appreciably and unsymmetrically affected fore and aft due to latent heat. This liberation at the rear becomes overpowering, with significant elongations of the tail of the pool as $\alpha \to \infty$, i.e., high velocity-power. Hence, a more appreciable nominal penetration decrement is experienced under these conditions. These facts have significant implications with respect to convection currents in the pool and nugget solidification. In

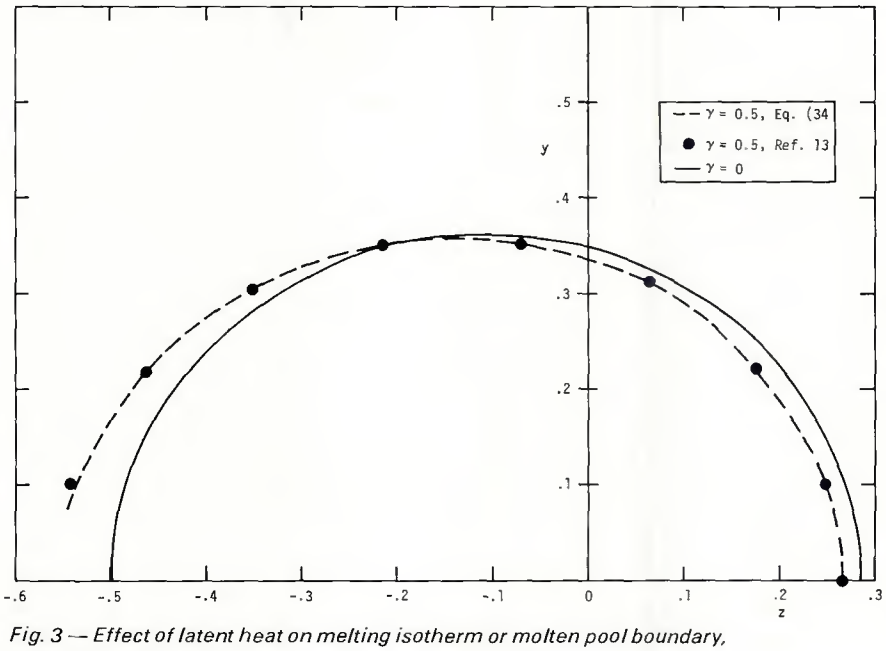

Fig. 3 — Effect of latent heat on melting isotherm or molten pool boundary, $\alpha = 0.5$, $\gamma = 0.5$

spite of the relatively small change in *nominal* penetration, *actual* penetration may be significantly affected by the rather appreciable elongation of the pool to the rear. This is particularly true from the standpoint of backwash currents eroding the edges of the nugget in the welding direction and forming the familiar dished-in profile.

A more dramatic effect on the pool contour is shown in Fig. 4 for $\alpha = 5$, where the latent heat elongates the tail in a more pronounced fashion than at $\alpha = 0.5$. There is a suggestion of a cusp behavior, which would agree with experimental observations. For practical interest, GTA welding conditions producing a value of $\alpha = 5$, assuming an efficiency of 80%, can be achieved with an input power of 5KW at approximately 20 ipm.

In Fig. 5, the effect of latent heat on the correlation in Ref. 3 is shown. There appears to be a small effect on penetration for the indicated α range — its magnitude growing as the speed-power parameter increases, i.e., $\tilde{\nu} = \alpha^{-1}$ decreasing. It should be noted that the effect is a nominal one, i.e., it pertains to the maximum displacement of the melting isotherm, δ, in units of λ ignoring convection in the pool. The large elongation due to latent heat will possibly induce important secondary effects on penetration. Moreover, the logarithmic plot makes the effect look smaller than it actually is, e.g., for $\alpha = 50$, the penetration decrement is of the order of 10%. Another factor increasing the decrement would be the substantially larger γ values associated with preheating, particularly in the case of low melting point materials such as tin and aluminum alloys. Lastly, values of γ of the order of ten times that assumed herein should markedly affect the vaporization contour.

GTAW Heat Transfer Efficiency

An important element in constructing the correlation of dimensionless penetration shown in Fig. 5 is the fraction of arc energy, η, entering the workpiece as heat. Although there has been considerable discussion of this problem in the literature, the significant work has been concerned primarily with the idealized case corresponding to nonmelting workpieces. The pioneering spectroscopic research of Olsen in Ref. 12 spawned these efforts, in which an apparatus was devised to insure a high degree of repeatability and stability. For this application, measurements over long time periods are required for the large quantity of data necessary to infer temperature distributions in the arc itself. Techniques developed by C. B. Shaw, Jr., of our laboratory, which reduce this data base requirement, are discussed in Ref. 13. Cooled anode heat transfer studies are typified by Refs. 14-17, in which dc straight polarity freely burning arcs have been investigated with ingenious continuous flow calorimetric devices which enable not only the integrated heat flux to be measured but its local intensity as well.

In practice, melting and vaporization are an important part of the energy budget. This is partially due to the significant latent heats associated with these phase changes, a fact that was pointed out earlier in this paper, and suggested in estimates given by Ecker in Ref. 18. Accordingly, there has been some consideration in the literature of melting

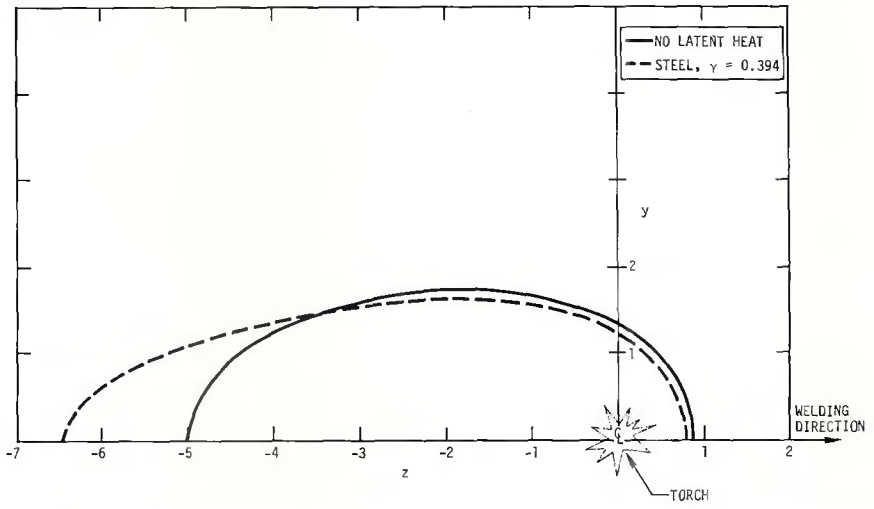

Fig. 4 — Elongation of molten pool produced by latent heat effect, $\alpha = 5$ for steel (axes moving with torch)

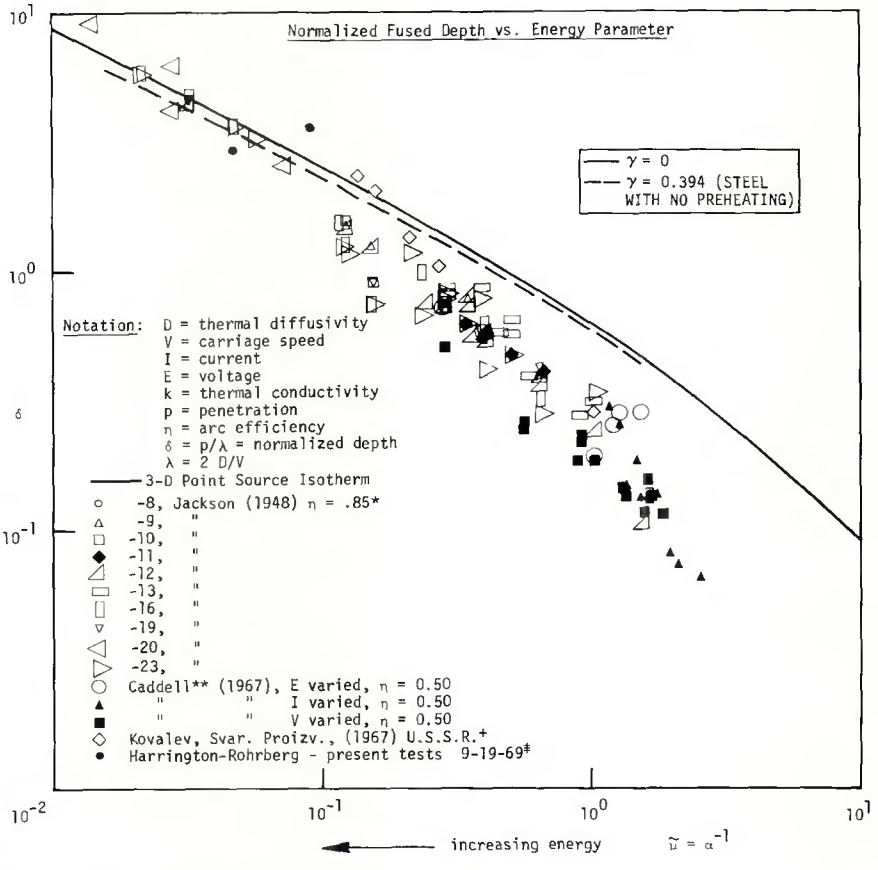

* submerged (unionmelt) and open arc
** consumable - open arc
\+ CO_2 jet welding - jets off, $\eta = .85$
‡ He jet welding - jets off, $\eta = .85$

Fig. 5 — Effect of latent heat on nominal penetration

anodes. Some of these studies use drop calorimetry and others employ continuous flow calorimeters. In the papers discussing these methods, few details are given concerning how important loss mechanisms are controlled or accounted for in the design and interpretation of the experiments. Moreover, there is a need for more information regarding the effect of various parameters on η for melting anodes. In what follows, a new calorimetric technique will be discussed, and some recent results obtained with the method will be presented for high conductivity materials.

"Dry" Calorimetry

The transient thermal response of the workpiece provides the basis for estimation of the heat transfer in the "dry" calorimetric method. In studying the feasibility of this concept, specimens were exposed to stationary arcs. For this case, a one-dimensional model for the heat balance proved to be a useful approximation for high conductivity materials. Letting $\bar{V}$, and S signify specimen volume and surface area respectively, with $\bar{t}$ = time, T_∞ = ambient temperature, h = Newtonian film cooling coefficient, Q = arc power delivered to workpiece, an elementary heat balance for the mean temperature $\bar{T}$ in the specimen gives:

$$Qh(\bar{t}-\bar{t}_o) = \rho c\bar{V}\frac{d\bar{T}}{d\bar{t}} + hS(\bar{T}-T_\infty) \qquad (5)$$

$$H(x) = 1 \quad \text{for} \quad x \geq 0$$

$$= 0 \quad \text{for} \quad x < 0$$

where the arc is struck at $\bar{t}=0$ and extinguished at $\bar{t}_o$, and the second term on the right hand side is a linearized approximation giving the combined effects of free and forced convection as well as radiation at moderate temperatures. In the application of the method, $T(0) = \bar{T}(0) = T_\infty$, where the unbarred T is the local temperature and $\bar{t}_o$ is selected to insure the validity of the Newton linear radiation law. The value of h is obtained from observation of $\bar{T}(\bar{t})$ for $\bar{t} \geq \bar{t}_o$. On introducing the characteristic thermal relaxation time,* $\tau = \frac{\rho cV}{hS}$, and an "equilibrium" temperature $\frac{Q}{hS}$, dimensionless quantities for the temperature and time may be advantageously introduced as follows

$$\theta = (\bar{T}-T_\infty)hS/Q \qquad (6a)$$

$$t = \bar{t}/\tau \qquad (6b)$$

The choice of these "lumped variables" eliminates explicit dependence of parameters such as Q, ρ, c, etc. and combines all the information into a "universal response" valid for varying materials, surface areas, etc. On substitution of (6) into (5), the problem for the normalized temperature becomes:

$$\frac{d\theta}{dt} + \theta = H(t-t_o) \qquad (7a)$$

$$\theta(0) = 0 \qquad (7b)$$

where it is understood that θ is continuous at t_o. The solution of (7) is

$$\theta = 1-e^{-t}, \qquad t \leq t_o \qquad (8a)$$

$$= (e^{t_o}-1)e^{-t} \qquad t \geq t_o \qquad (8b)$$

To assess η, the universal function (8) was applied to reduce the observed thermal response of billet shaped specimens with thermocouples mounted on the axis of symmetry as shown in Fig. 6. A ground clamp was mounted in the manner indicated to insure axial symmetry. Heat loss to this device was suppressed by minimizing the contact area. In addition, ohmic heating losses in the specimen were estimated to be negligible. Factors affecting the repeatability include electrode alignment and shape. Very small variations of the tungsten tip produced marked discrepancies in the runs. For assessment of the nominal arc power, the voltage drop across the arc was measured. The amperage-voltage characteristic curve qualitatively resembled data given in Ref. 19 for carbon arcs, and Ref. 20 for argon discharges.

In Fig. 7, experimental data for 6061 aluminum alloy are compared with the theoretical response curve from (8) using the normalized variables. The procedure here was to determine h and η to provide the best fit of the experimental data with (8). The arc extinction time $t=t_o$ is shown as the dashed line. The agreement is excellent in this case showing the potentialities of the method for estimating η for high conductivity workpieces.

A similar comparison for 304 stainless steel shown in Fig. 8 indicates poorer agreement. This is partially due to the breakdown in the assumptions of one-dimensionality inherent in (8), i.e., the thermal conductivity and diffusivity are so low that temperature gradients are no longer "smeared out."

Another factor influencing the quality of agreement is the nonlinear effect of thermal radiation. This effect is manifested at higher power inputs and can be expressed in terms of a characteristic time scale which can be estimated from a refinement of (5) which includes a radiation term. A discussion of these corrections will be given in a future publication, which will provide a comparison of a three-dimensional unsteady model with experimental results for lower conductivity materials, typified by ferrous and nickel based alloys. For purposes of the present discussion, it will be sufficient to indicate that nonlinear radiative cooling can be neglected in the dry calorimetry method over a range of conditions specified in terms of certain dimensionless parameters, which are expressed in terms of ϵ, the radiative emissivity, and σ the Stefan-Boltzmann constant

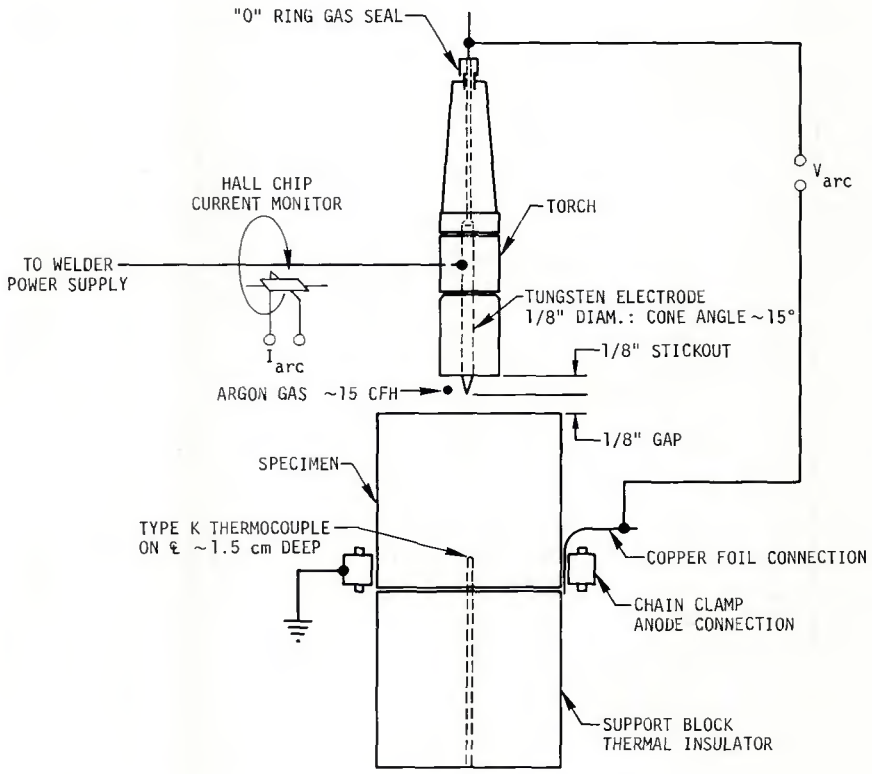

Fig. 6 — Schematic of dry calorimetric apparatus

**This is a measure of the time it would take a hot body to cool to ambient temperature, with Newtonian cooling.*

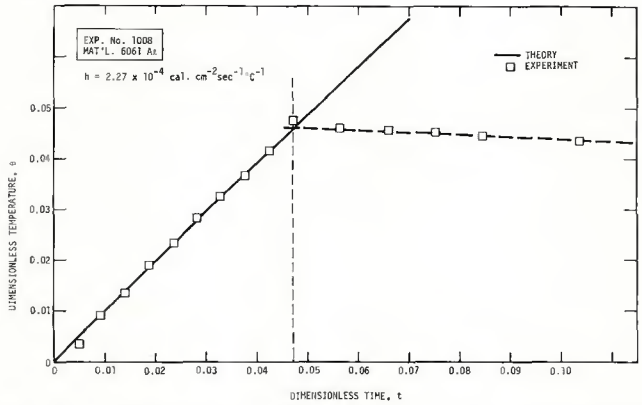

Fig. 7 — Dimensionless thermal response curve for 6061 aluminum

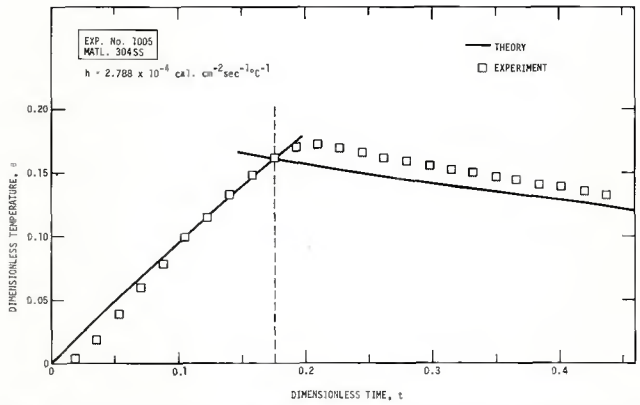

Fig. 8 — Dimensionless thermal response curve for 304 stainless steel

appearing in the Stefan radiation law. These parameters, A and B are given by the formulas:

$$A \equiv \sigma\varepsilon Q^3/h^3 S^3 \quad , \quad B \equiv hS\bar{T}_\infty/Q$$

and the linearity condition can be expressed as

$$6AB^2 t/(1+4AB^3) << 1 \qquad (9)$$

From these relations, it is possible to design experiments which suppress radiation effects and thereby simplify the inference of η from the specimen transient response. In this manner, weldability of new materials as influenced partially by the magnitude of η could be determined relatively inexpensively. It should be emphasized that the procedure assumes moderately high diffusivities. For application to automatic welding, a further assumption must be made regarding negligible effects associated with convection processes attributed to relative motion of the torch and workpiece. The last assumption should be valid for low travel speeds.

Associated with lower conductivity metals, another important factor is responsible for discrepancies between the theory and experiment as shown in Fig. 8. This pertains to the "rounding" effect of the thermal response curves associated with the increased time required for temperature gradients to diffuse into the work. The time scale, t_D of these "fillets" on the response curve is of the order of ℓ^2/D, where ℓ is a characteristic workpiece dimension, and D is the thermal diffusivity. Such fairings smooth out the arc switch-on and switch-off transients occurring at $t=0$ and $t=\bar{t}_o$ in the curves of Figs. 7 and 8. In the application of the dry calorimetry method to high conductivity metals, the inference of η from thermal response is therefore most easily affected when the dimensional switch-off time, $\bar{t}_o$ is in the linear range given from previous considerations as

$$C\ell^2/D < \bar{t}_o << D\rho cV(Q^3\sigma\varepsilon S)^{-1/4}$$

C,D ≡ dimensionless constants

Whereas high conductivity metals can be fairly well characterized by an average temperature in the linear region, lower conductivity materials exhibit significant spatial variations in this range. However, a property of the three-dimensional theoretical solution which predicts these variations is that the *slope* of the time-temperature curve is identical for different points in the specimen in a so called "linear asymptote" region, which is established for sufficiently long times, short of those for the initiation of significant radiation effects. These slopes can then be used to determine η for moderate power inputs.* In the remaining part of this discussion, only the high conductivity case will be considered.

To illustrate the validity of the theoretical scaling law predicted on the assumption of the average temperature model intrinsic in Eq. (8), a dimensionless universal heating curve is shown in Fig. 9a. It is evident that during the time scale selected, the normalized response is a nearly linear function of temperature for the three different materials selected. The corresponding curve for cooling response is shown in Fig. 9b. In both figures, the values of h and η in the individual experiments were determined as those giving the best possible fit of these universal curves.**

The results of the measurements of η for 6061 Al as a function of current for a stationary 1/8 in. tungsten, 15 deg cone angle electrode with a work to cup distance of 1/4 in. using a pure argon shield gas is shown in Fig. 10. For the current range indicated, it is apparent that the efficiency is relatively constant. A similar invariance is indicated for arc lengths between 1 to 3 mm. The comparison shown with Lancaster's data of Ref. 17 indicates surprising agreement. Results of Nestor in Ref. 14, and Wilkinson and Milner in Ref. 16 indicate somewhat higher orders of magnitude for η, than those shown. Both workers quote values of 90% or above for similar argon shielded arcs, but with water cooled anodes appropriate to their continuous flow calorimetric devices. Nestor reported an invariance of heat transfer at 90% efficiency over a range of arc pressures from 195 mm to 790 mm Hg. The higher values of the water cooled anode results of Ref. 14 and 16 are plausible due to the elimination of energy loss mechanisms such as those due to change of state appropriate to the results of this paper.

As an additional validation of the measurements. continuous flow calorimeters were employed which allowed surface melting and vaporization. These measurements are also shown in Fig. 10 and compare favorably with the dry calorimetric results. Both block and hemispherical shaped devices were used to obtain these data.

The values of η obtained in these experiments were used in a comparison of point and line source theory against measured thermal cycles in bead on plate welds in thin and thick plates. Such studies gave reasonable agreement for the cases considered. From these indications, it appears that the dry calorimetric concept offers a relatively cheap and simple method for obtaining a quick assessment of heat transfer efficiency as an input for welding process-thermal cycle predictions. Future efforts will be devoted toward obtaining the influence of electrode configuration,† shield gas flow rate, and composition on η.

**Because of nonlinear radiative effects at larger power inputs, no linear asymptote region will be obtained, and η must be obtained by matching the initial "switch on" transient of the linear theory with the observations.*

***Note the relatively small spread in the value of* h.

† Interesting studies of electrode effects on bead width and penetration are given in Refs. 21 and 22.

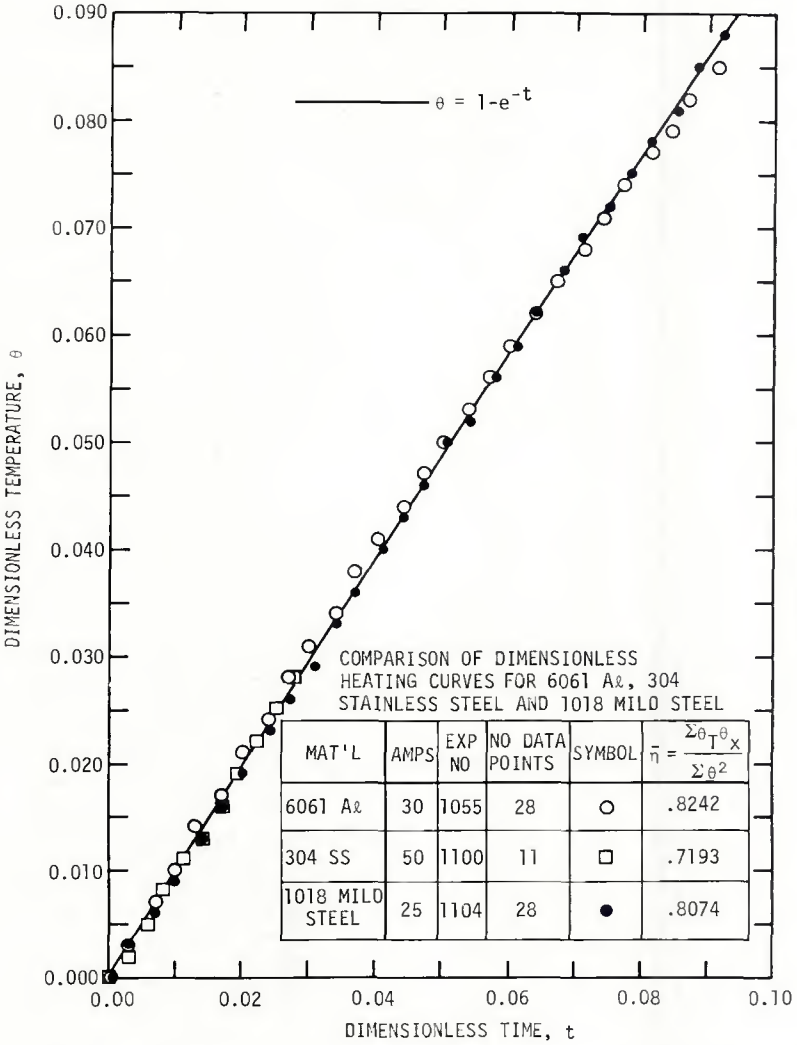

Fig. 9a — Universal heating response curve for dry calorimetric experiments

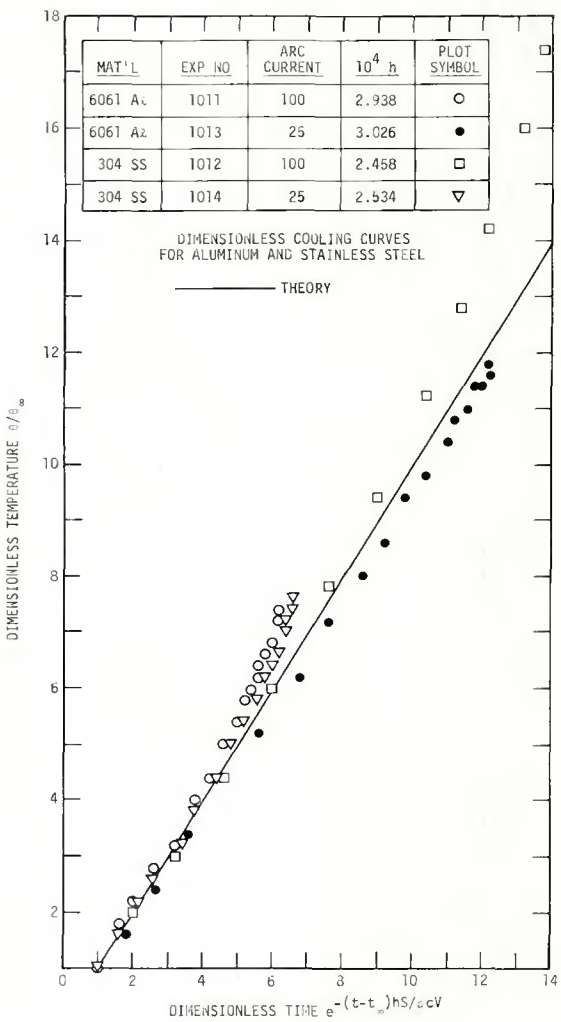

Fig. 9b — Universal cooling response curve for dry calorimetric experiments

Backing Effects

A significant factor in the evolution of thermal patterns in welding is the influence of boundary conditions. Roberts and Wells in Ref. 23 gave estimates for bounding plane effects and made recommendations concerning when the simpler isolated source models provide a good approximation to the more complicated expressions which account for finite boundaries. These results were chiefly for temperatures along the line of welding, on insulated plates. Aside from this effort and some empirical studies, it appears that the subject of boundary conditions has been slighted in the welding literature.

This is unfortunate, since fixtures which include such elements as hold downs, clamps, and backing bars, can produce decisive changes in thermal patterns in the workpiece, thereby affecting weld nugget geometry, solidification mechanics and mechanical properties. Furthermore, it is probable that these variables may be controlled and optimized through the proper design of such fixtures. Toward achieving these goals, a self-consistent mathematical theory can be of use in identifying important parameters, and in the prediction of perturbations of the thermal field associated with fixture elements. Such a model applicable to backing effects will be discussed in what follows within the context of a new validating experimental technique.

Theory

For purposes of simulating the influence of backing bars, the configuration shown in Fig. 11 is considered. The workpiece denoted by (1) in the figure is placed in contact with a backing (2) of different thermal properties. Without undue loss of generality, it will be assumed that the base of the backing bar and the vertical sides parallel to the line of welding are sufficiently distant to render their influence on the thermal pattern negligible.* With the axis convention shown, the problem can be then idealized as the temperature field associated with the thermal field of a moving point source on a slab (1) with auxiliary boundary conditions at the interface between (1) and (2) at $z = \ell$. If contact resistance at the interface is neglected, † these auxiliary conditions are

$$k_1 \frac{\partial \bar{T}_1}{\partial z} = k_2 \frac{\partial \bar{T}_2}{\partial z} \qquad (10a)$$

$$T_1 = T_2 \qquad (10b)$$

at $z=\ell$, where subscripts 1 and 2 refer to the plates (1) and (2) respectively. In addition to these relations, it is assumed that the arc is struck at $x=x_o$ on the x axis at $t=0$, and forward motion at the travel speed v is initiated at that instant. The solution of this unsteady three dimensional heat conduction problem has been obtained using transform calculus and leads to rather complicated looking analytical expressions. An adequate discussion of these would lead far beyond the scope of this paper. How-

**A more realistic model including the effect of the vertical side planes is discussed in Appendix 1.*

†Recent tests indicate that this assumption is a good approximation in many cases of practical interest.

ever, a considerable simplification can be realized by the use of further approximations. These are made in the context of correlation of the thermal pattern on the plane $x=0$ with the conditions in a plane moving with the arc. For this purpose, it should be noted that the unsteady pattern observed in the plane $x=0$ consists of two time dependent effects: 1) that due to the switch-on of the arc at $t=0$, with related conduction transients, as well as 2) a "steady-state" transient associated with a receding pair of vertical source arrays moving in opposite directions at the torch speed v along the x axis, where the image system traveling in the negative x direction is required to satisfy assumed insultated conditions on $x=0$. Analytical estimates indicate that for all but small times after arc initiation, effect (1) is negligible compared to (2). Furthermore, it is useful to consider two limiting cases: (i) $\mu \equiv \frac{k1}{k_2} \to 0$ (insulated), and (ii) $\mu \to \infty$ (perfectly conducting). These cases bracket the results and give qualitative indications of certain features of the finite μ problem. Case (ii) is an approximation appropriate to a copper backing bar in contact with a material of much lower conductivity, such as steel, leading to a value of μ of the order of 10. It can be shown that this approximation is also valid when the heat capacity parameter $\nu \equiv \ell\rho c/Mc'$ is $\ll 1$, where c and c' are specific heats of the work and backing respectively, and M is the mass of the backing per unit area at the plane of contact. Letting α = thermal diffusivity, T_∞ = ambient temperature, x_o = arc's initial position at $t=0$, Q = arc power delivered to workpiece, T_m = melting temperature and referring to the Cartesian axis system shown in Fig. 11, the following quantities are defined

$$\lambda \equiv 2\alpha/V,\ \xi \equiv (x-x_o-Vt)/\lambda,\ \eta \equiv y/\lambda,$$
$$\rho^2 \equiv \xi^2 + \eta^2$$
$$\zeta \equiv z/\lambda,\ \tau^* \equiv \ell/\lambda,\ u \equiv 2\pi k_1 \lambda (T-T_\infty)/Q\ .$$

For cases (i) and (ii) above, the dimensionless temperature distributions, u for an infinitely long plate in the x direction are:

$$u = \frac{e^{-\xi}}{\tau^*}\left\{K_o(\rho) + 2\sum_0^\infty K_o\left[\rho\left(1+\left(\frac{n\pi}{\tau^*}\right)^2\right)^{\frac{1}{2}}\right] \times \cos\frac{n\pi\zeta}{\tau^*}\right\},\ \mu \to 0 \qquad (11a)$$

$$u = \frac{2e^{-\xi}}{\tau^*}\sum_0^\infty K_o\left[\rho\left(1+\left|\frac{(2n+1)\pi}{2\tau^*}\right|^2\right)^{\frac{1}{2}}\right] \times \cos\frac{2n+1}{2}\frac{\pi\zeta}{\tau^*},\ \mu \to \infty \qquad (11b)$$

where the symbol K_o signifies the modified Bessel function of zeroth order. The Fourier-Bessel series of Eqs. (11) converge rapidly for moderately small τ^*. For larger values of τ^*, the following image series are rapidly converging alternative representations:

$$u = e^{-\xi}\sum_{-\infty}^{\infty}\frac{e^{-\rho_n}}{\rho_n}, \qquad (12a)$$

(source series), $\mu \to 0$

$$u = e^{-\xi}\sum_{-\infty}^{\infty}(-1)^n\frac{e^{-\rho_n}}{\rho_n}, \qquad (12b)$$

(source-sink series), $\mu \to \infty$

where $\rho_n^2 \equiv \rho^2 + (2n\tau+\zeta)^2$. Eqs. (11a) and (12a) were first derived in Ref. 2. Neglecting the influence of the end plane perpendicular to the line of welding at the far end,** the dimensionless temperature, $\tilde{u}$ accounting for the effect of the insulated boundary, $x=0$, can be expressed using an image system "reflected" in the $x=0$ plane as

$$\tilde{u} = \phi(x,y,z,t;V,x_o) + \phi(-x,y,z,t;V,x_o)$$

where ϕ corresponds to any of the solutions of (11) or (12). Accordingly, the temperature $\tilde{u}$ at $x=0$, taking into account the $x=0$ end effect is just

***This is a good approximation for plates of typical lengths encountered in practice.*

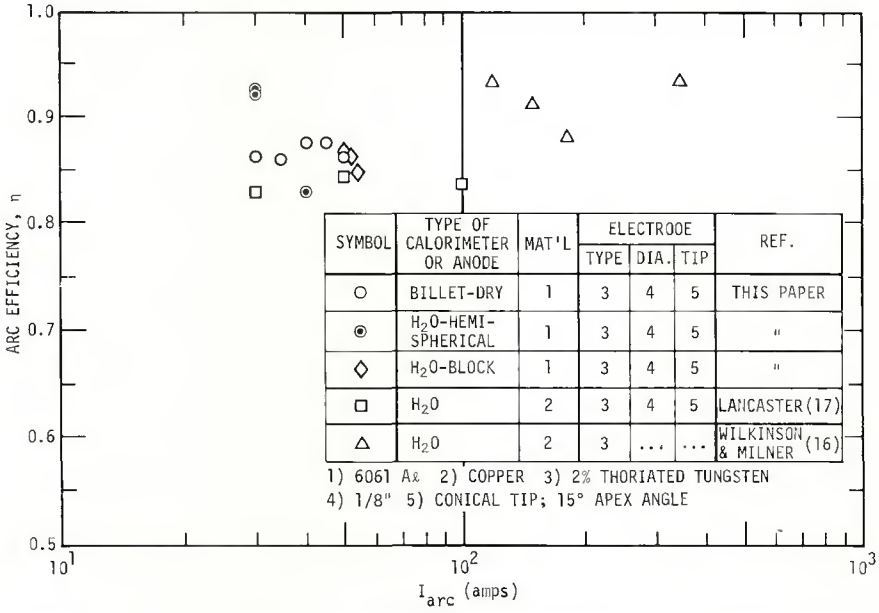

Fig. 10 — Comparison of dry calorimetric data on melting anodes with published results for cooled anodes

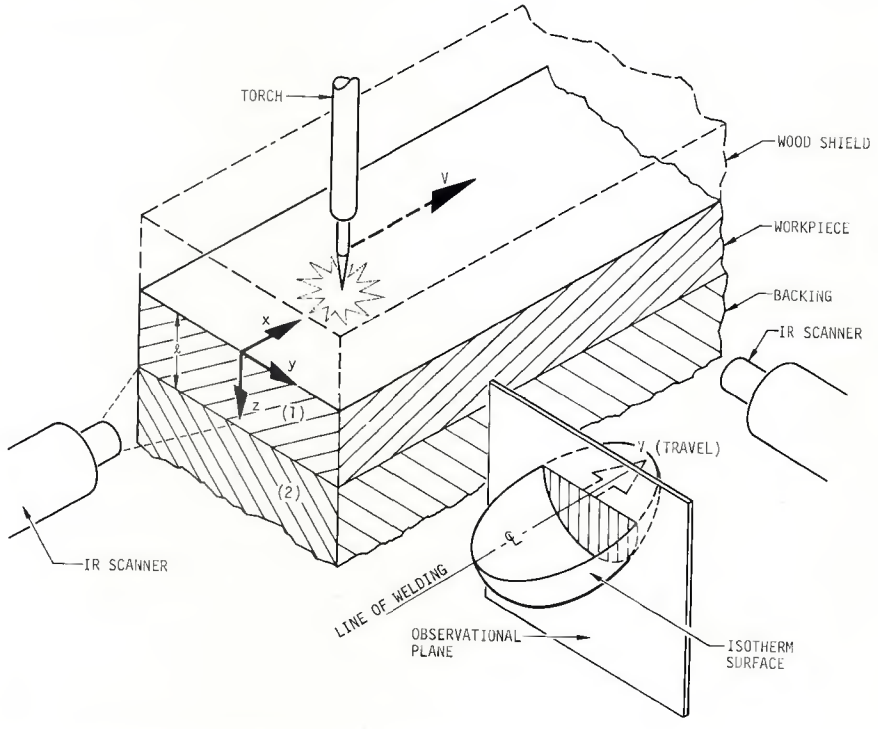

Fig. 11 — Backing bar configuration and isotherm motion

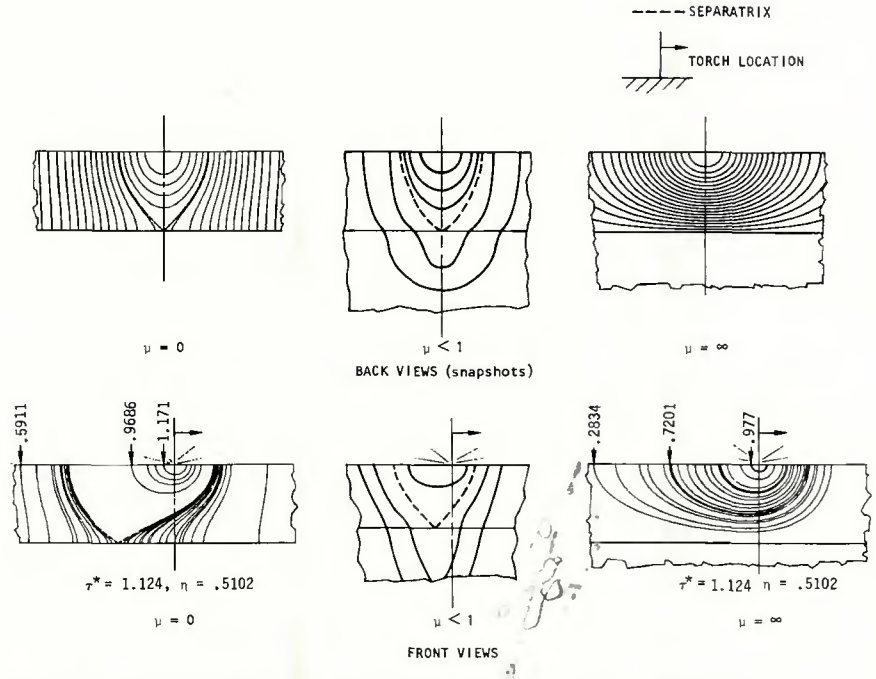

Fig. 12 — Isotherm configurations for limiting and intermediate backing cases

twice any of the formulas in (11) and (12). In the inset of Fig. 11, a typical egg-shaped isotherm surface near the line of welding is shown as it recedes into a plane, x = constant, perpendicular to this line. The trace of intersection of this surface with the plane is shown as the shaded area whose boundary is a typical isotherm "snapshot." To an observer fixed with respect to the plane, the successive isotherm positions will shrink into the pierce point 0 of the weld line and the observational plane, i.e. the (y,z) origin, as time increases. Calculations based on Eqs. (11) and (12) lead to the isotherm snapshots shown in Fig. 12; or the limiting cases $\mu=0$ and $\mu=\infty$, corresponding to a back view (observational plane perpendicular to line of welding) and side view (in a vertical plane parallel to line of welding). A qualitative sketch of the case $\mu<1$ is also shown. Relatively simple reasoning can be used to obtain these intermediate and limiting patterns. Thus, near the point 0, the isotherms will approach the egg shaped pattern from an isolated point source.† The other characteristics can be deduced from the fact that the slope $(dz/dy)_I$ of an isotherm curve in a plane x = const. is given by:

$$\left(\frac{dz}{dy}\right)_I = -\,(\partial T/\partial y)/(\partial T/\partial z) \qquad (13)$$

On the centerline in the back views, $\partial T/\partial z = 0$ by symmetry, and since $\partial T/\partial y$ will be zero only at exceptional points, the level curves are horizontal along this line. From Eqs. (10) and similar reasoning, it is evident that aside from singular points, the isotherms will be normal or parallel to the bottom surface for the cases $\mu=0$ and $\mu=\infty$, respectively. For the intermediate case $\mu<1$, Eq. (10a) indicates that there will be a kink in the isotherms at the interface. An important feature of each of the patterns is the presence of a separatrix (shown as dashed lines) which, in the back view, divides curves which intersect the centerline from those that intersect the bottom surface $z=\ell$. In the back views, the separatrix emanates from the intersection of the centerline and the bottom surface which is a singular point, i.e., where both the numerator and denominator in the right hand side of (13) vanish.

Analogous reasoning can be used to deduce the side view patterns shown. Far from the separatrix, the isotherms correspond to those for a thin plate ($\overset{*}{\tau}\to 0$) irrespective of the values of μ and the dimensionless thickness, $\overset{*}{\tau}$. On the other hand, the pattern close to the source corresponds to that for an infinitely thick plate ($\overset{*}{\tau}\to\infty$). A deeper significance of the separatrix is that the value of temperature it carries has a decisive effect on nugget geometry. Denoting T_s as the separatrix temperature, the two cases $T_s \ll T_m$ and $T_s \gg T_m$ give radically different nugget shapes as is evident from Fig. 12. All other factors such as electrode shape, shield gas, etc. remaining the same, the occurrence of these situations will depend on the magnitude of $\overset{*}{\tau}, \mu$ and the dimensionless power parameter α introduced previously. For a fixed μ and α, the occurrence of parallel wall, hour glass, and semicircular weld nuggets for arc anode interactions roughly correspond to $\overset{*}{\tau}\ll 1$, $\overset{*}{\tau}\sim 1$, and $\overset{*}{\tau}\gg 1$, respectively, in the same manner as described in Refs. 4 and 5 for laser welding. Moreover, such considerations are relevant to the studies of Refs. 13, 21 and 22.

On comparison of the side view isotherms for $\mu=0$ and ∞ given in Fig. 12* for the same $\overset{*}{\tau}$, and α, it is evident that the perfectly conducting case leads to the anticipated lower temperatures than the insulated one for the same power input. It is also evident that there is a radical change in the pattern, and the effect of this change on the nugget geometry could be important, depending on the value of α. This fact suggests the possibility of controlling nugget configuration by judicious selection of the parameters μ and α, to satisfy specific service requirements.

IR Thermography in Welding

To validate the theoretical predictions, it was necessary to devise a practical method of observing the temperature contours. Thermocouple techniques provide useful information on temperature levels, but because of practical problems such as their interaction with the measurements, they can not be employed in sufficient numbers to afford the spatial resolution necessary for developing reliable temperature patterns. For satisfying this need, the feasibility of modern infrared (IR) sensing units was investigated. Although IR detectors have been available for some time, only recently have systems become available which provide continuous monitoring of areas with sufficient spatial and temporal resolution to be of use for welding thermal studies. One such system having a vidicon scanner and cinematographic attachments was used to observe isotherm development associated with backing effects.

Color movies showing transient temperature response under a variety of conditions have been obtained, using special close-up lens attachments and the shield configuration shown in Fig. 11. Black and white versions of typical stills are shown in Figs. 13-15. Because this investigation was restricted to establishing feasibility of the experimental methods, a primarily qualitative comparison with theory will be discussed in what follows. The quantitative resolution will be deferred to another publication.

Figures 13a and 13b show typical

†*This remark applies for small enough times such that a subsequently defined curve, termed the "separatrix," is in view. For larger times, all of the isotherms will be nearly straight lines perpendicular to upper and lower surfaces, as in the "thin plate" regime.*

Footer: 396-s | SEPTEMBER 1974

**In the end views of Fig. 12 no attempt was made to keep α and τ^* fixed for the cases shown.*

snapshots of the isotherm pattern on a vertical face of a 3-1/8 × 3-1/16 × 16 in. 2014 T6 Al workpiece, parallel to the line of welding for GTAW at 6 and 12 ipm at 200A and 12V. The general features agree closely with those shown for $\mu=0$ in Fig. 12 and Ref. 2, representing to our knowledge the first verification of these distributions. In these and subsequent figures, the various hues represent preassigned increments in temperature appropriate for the temperature range to be considered, with temperature increasing from left to right in the legend. A calculation using the more elaborate expression (A1) in Appendix 1, and a contour plotting routine is shown in Fig. 13c as well as the overlay of Fig. 13d**. Qualitative agreement is encouraging although some quantitative discrepancies are present, possibly due to the influences of end planes and radiation.

Backing bar effects are shown in the end views of Figs. 14a and 14b. These tests were run on a 12 × 4 in. 1018 mild steel workpiece for ½ and 1 in. thicknesses respectively, at 100 A, 12 V, at 3 ipm using typical argon shielded GTA equipment. In (14a), the thin piece exhibits the rounding effect on the isotherms associated with a large value of μ, and a coincidence of the interface with the ambient tem-

**The level lines selected in the routine correspond to the observed values.*

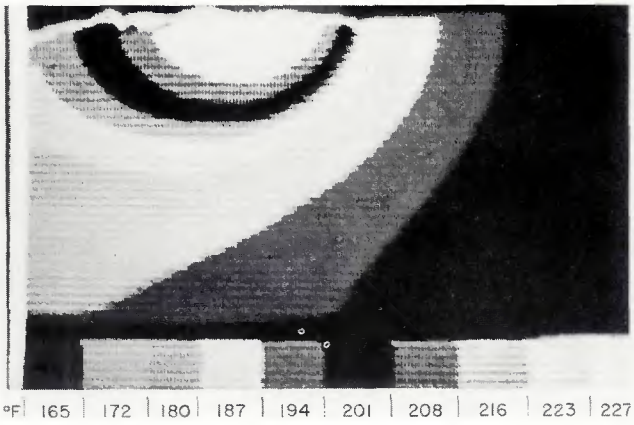

Fig. 13a — IR side view of isotherm pattern (V = 6 ipm)

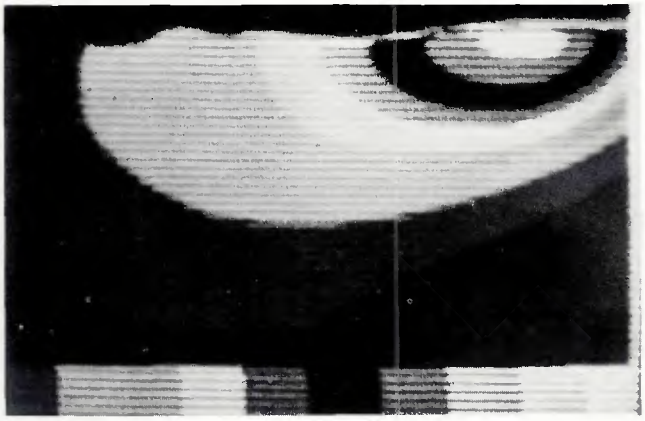

Fig. 13b — IR side view of isotherm pattern (V = 12 ipm)

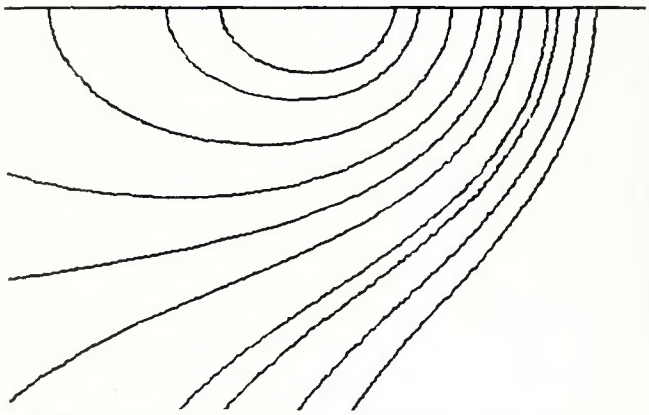

Fig. 13c — Computed normalized isotherms corresponding to Fig. 13a

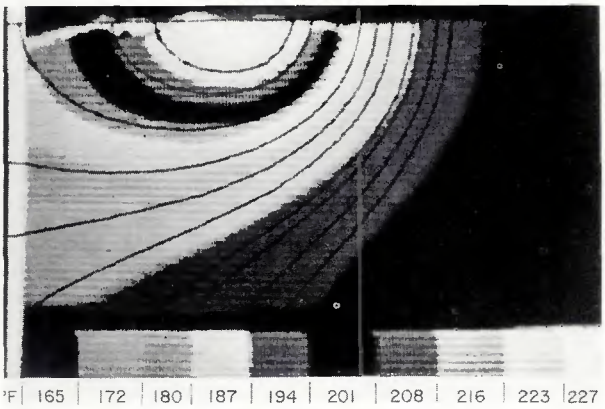

Fig. 13d — Overlay of Figs. 13a and 13c

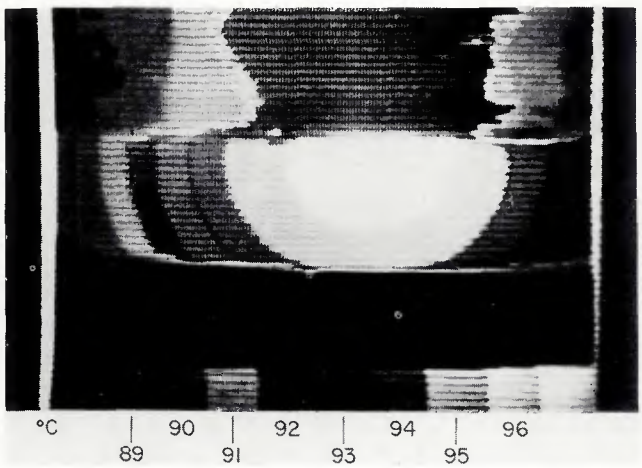

Fig. 14a — Effect of Cu backing on IR end view of isotherm pattern — thin piece

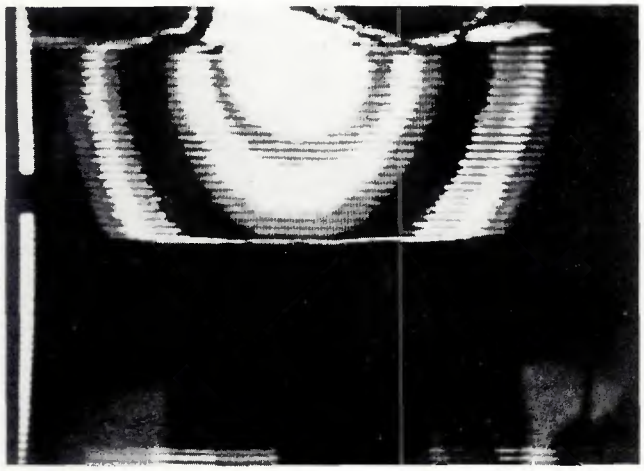

Fig. 14b — Effect of Cu backing on IR end view of isotherm pattern — thick piece

perature level line, in agreement with the discussion of the previous section. For (14b), the pattern is in accord with the $\mu<1$ sketch shown in Fig. 12. By use of a thermocouple, the relative intensities were correlated with the temperature levels shown on the bar legends in Figs. 14 and 15. The latter depicts an end view of a $\mu=0$, 1 in. thickness case with all other conditions identical to those just described. The pattern shows the anticipated stretching in the vertical direction associated with normality of the isotherms on the lower surface. This stretching is confirmed by a corresponding comparison of macrosections shown in Figs. 16a and 16b, and agrees with conclusions of Shaw in Ref. 13.

Using these tools, the possibility of monitoring thermal cycles during actual operations appears attractive. Through theoretical developments such as Eqs. (11) and (12), events on an observational plane perpendicular to the line of welding can be correlated with the linear envelope of the receding isotherm surface, which determines HAZ and fused zone configurations. In this manner, undesirable characteristics can be quickly modified or even corrected using closed loop controls. As an illustration, the techniques described were effective in distinguishing gaps and improper fit-up due to warpage in fixtures for multiple pass welds. These problems were detected from abnormal asymmetries in the evaluation of end view isotherm patterns as the torch receded away from the observational plane. Another application of the system could be in the determination of optimum weld parameters and fixtures to achieve desired penetration characteristics. Beyond these examples, the technique should provide further information in the enhancement of fundamental knowledge concerning the physics of welding.

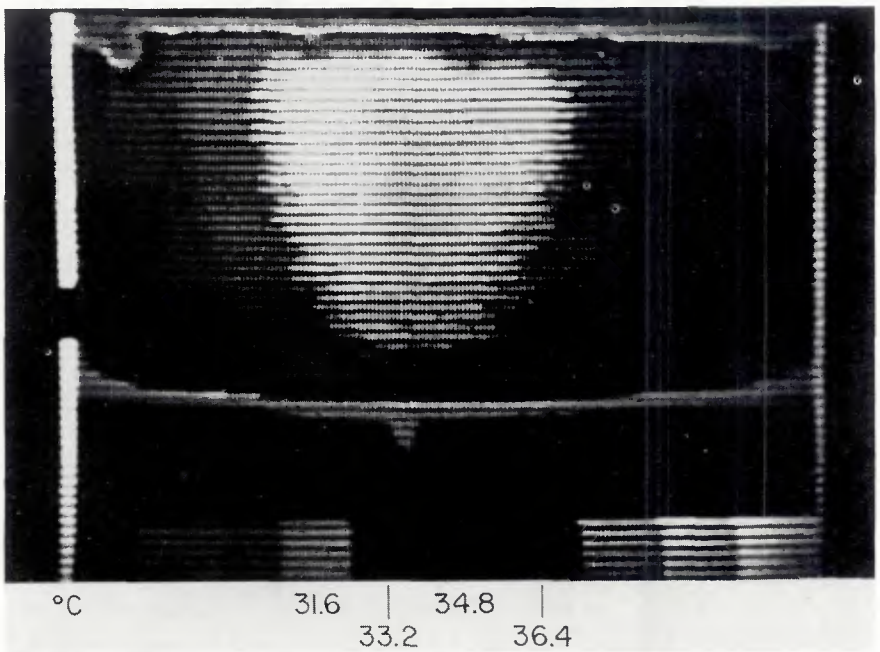

Fig. 15 — Backing absent — IR end view of isotherm pattern — thick piece

Conclusions

Three areas were investigated to provide information regarding thermal processes in welding. In the first, the effect of accounting for the latent heat of fusion in an isolated point source simulation of the GTAW process was considered. From nonlinear heat conduction theory and perturbation methods, a self consistent approximate mathematical solution for this correction has been presented. Predictions using the formula show that the effect has a relatively unimportant influence on "nominal" penetration, i.e., maximum width of the point source melting isotherm. However, it induces drastic elongations in the pool at moderate travel speeds and power levels, which may be important in changing the bead geometry through attendant modification of convection and subsequent recrystallization patterns in the melt.

The second area considered pertains to heat transfer efficiency, η of welding arcs. A "dry" calorimetric concept has been discussed which provides a relatively simple, quick, and inexpensive method for obtaining performance of various arcs. Experimental data from this method indicate that η is invariant with current over a range of 30-50 A, in a stationary GTA arc on 6061 Al, for a thoriated, tungsten, 15 deg taper angle, electrode. For the same workpiece material, there is also an invariance in η with gap variation over a range of 1-3 mm. A comparison with published data for cooled anodes confirms the expectation that the efficiencies associated with the latter are somewhat higher than the results herein. Moreover, similar invariances are apparent in connection with non-

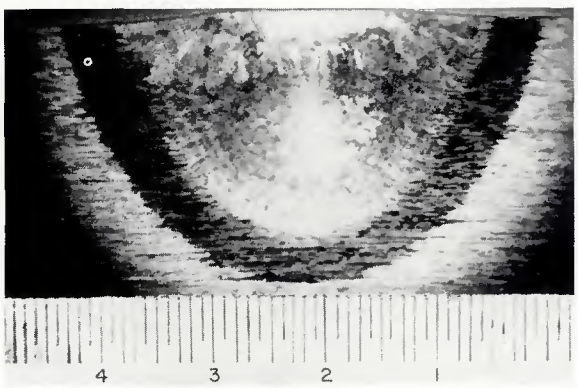

Fig. 16a — Macrophotograph showing HAZ and nugget — Cu backing

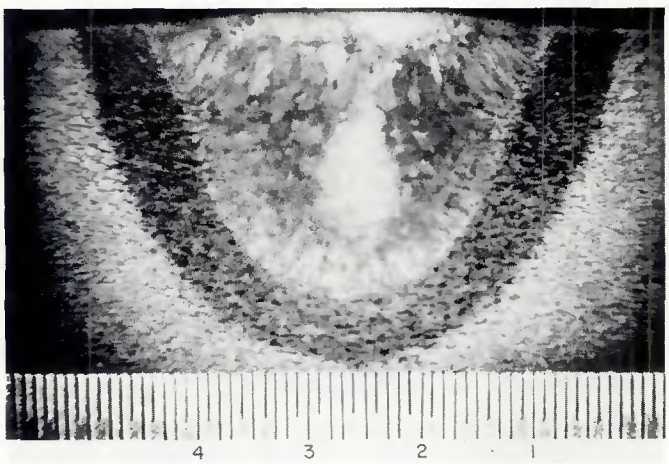

Fig. 16b — Macrophotograph showing HAZ and nugget — no backing

melting anodes. As an additional validation of the technique, continuous flow calorimetric measurements were performed. The results compare favorably with those obtained using the "dry" calorimetry method.

Effects of backing bars and the development of relevant theoretical solutions and experimental techniques were the last subject considered in the foregoing discussion. Solutions have been provided which bracket the effects between insulated and perfect conductor cases. The latter is a valid approximation for high conductivity backing when either the previously defined dimensionless heat capacity parameter, ν or conductivity ratio, μ, is small. The intermediate case of $\mu<1$ is discussed in Appendix 2. For validation of these solutions, and many other welding applications, the feasibility of IR thermography has been demonstrated. The technique qualitatively confirms isotherm patterns obtained from the $\mu=\infty$ limiting solution, the Rosenthal $\mu=0$ solution, as well as the intermediate case of $\mu<1$. Future effort will be devoted to exploiting this tool for applications in weld quality control, and more quantitative fundamental studies, using the theory as a guide in experimental design.

Acknowledgments

This work was performed under the Rockwell International Interdivisional Technology Program ITP6-Task 2 under the auspices of the Corporate Welding Technical Panel. The authors wish to acknowledge the stimulating interaction and encouragement of Charles B. Shaw, Jr., who has been an invaluable colleague since the project's inception. We also thank Welding Panel personnel, Norman Wilson and J. J. Halisky, Panel Chairmen and Project Coordinators, for their guidance and support, as well as A. H. Muir, Jr. The participation of B. McGuire, who was the IR thermographer, J. C. Gysbers and E. R. Cohen, who performed some of the numerical calculations, as well as Harry May, Harry Pontius, Ken Billington and John Curnow, who also assisted in the experiments and photography is also acknowledged. We are also grateful to Arthur Billy and Henry Tong for their comments at the outset of the effort. Finally, a portion of the research was performed under the IR&D program at the Science Center, and the authors wish to acknowledge the support of T. L. Loucks, C. J. Meechan, T. Wolfram and D. O. Thompson in this regard.

References

1. Jackson, C. E., "The Science of Arc Welding," *Welding Journal,* 39, (4), 1960, Research Suppl., 129-s to 190-s.

2. Rosenthal, D., "The Theory of Moving Sources of Heat and Its Application to Metal Treatments," *Transactions of the ASME,* 68 (11), 1946, 849 to 866.

3. Malmuth, N. D., "Arc Welding Research," Part I, North American Rockwell Science Center Technical Report, SCTR-69-30, 1969.

4. Malmuth, N. D., "Transient Thermal Phenomena in Moving CW Laser Irradiated Metallic Targets," (in press), to appear in *Proc. 1973 DoD Laser Effects/Hardening Conference.*

5. Malmuth, N. D., "Conduction Dominant Laser Irradiation of Metallic Materials," presented at the AIAA 8th Thermophysics Conference, July 16-18, 1973, Riviera Hotel, Palm Springs, California.

6. Christensen, N., Davies, V. de L., and Gjermundsen, K., "Distribution of Temperatures in Arc Welding," *British Welding Journal* 13 (2), 1965, 54 to 75.

7. Carslaw, H. S. and Jaeger, J. C., *Conduction of Heat in Solids 2nd ed.,* Oxford at the Clarendon Press, London, 1952, Chap. XI.

8. Goodman, T., "The Heat Balance Integral and Its Application to Problems Involving a Change of Phase," *Transactions of the ASME,* 80 (2), 1958, 338 to 342.

9. Cole, J. D., *Perturbation Methods in Applied Mathematics,* Blaisdell, Waltham, Mass., 1968.

10. Malmuth, N. D. and Hall, W. F., "Influence of Latent Heat of Fusion on the Temperature Field of a Moving Point Source," North American Rockwell Science Center Technical Report, SCTR-72-3, 1972.

11. Cohen, E. R., "The Melt Boundary in Arc or Electron Beam Welding," North American Rockwell Science Center Technical Report SCTR-72-4, 1972.

12. Olsen, H. N., "Thermal and Electrical Properties of an Argon Plasma," *Physics of Fluids,* 2 (12), 1959, 614 to 623.

13. Shaw, Jr., C. B., "Diagnostic Studies of the Welding Arc," presented at the 54th AWS Meeting, Chicago, Ill., April 2-6, 1973.

14. Nestor, O. H., "Heat Intensity and Current Density Distribution at the Anode of High Current, Inert Gas Arcs," *Journal of Applied Physics,* 33 (5), 1962, 1638 to 1648.

15. Shoeck, P., "An Investigation of Anode Heat Transfer in High Intensity Arcs in Argon," Ph.D. Thesis, 1961, University of Minnesota.

16. Wilkinson, J. B. and Milner, D. R., "Heat Transfer from Arcs," *British Welding Journal,* 8 (2), 1960, 115 to 128.

17. Lancaster, J. F., "Energy Distribution in Argon Shielded Welding Arcs," *British Welding Journal,* 2 (9), 1954, 412 to 426.

18. Ecker, G., "Electrode Components of the Arc Discharge," *Ergebnissen Der Exaten Naturwissenshaften,* 33, Springer Verlag, 1961, 1 to 104.

19. Cobine, J. D., *Gaseous Conductors,* Dover Publications, New York, 1958.

20. Olsen, H. N., "Temperature Measurements in Hugh Current Arc Plasmas," Paper presented at the 10th Annual Gaseous Electronics Conference, New York, October 2, 1957, (Abstract in *American Physical Society Bulletin,* pp. 81, January 29, 1958).

21. Savage, W. F., Strunk, S. S. and Ishikawa, Y., "The Effect of Electrode Geometry in Gas Tungsten-Arc Welding," *Welding Journal,* 44 (11), 1965, Research Suppl., 489-s to 496-s.

22. Spiller, K. R., and MacGregor, G., "Effect of Electrode Vertex Angle on Fused Weld Geometry in TIG Welding," *Proc. of the Conference on Advances in Welding Processes,* 14-16 April 1970, The Welding Institute, Abington Hall, Cambridge 1971.

23. Roberts, D. K. and Wells, A. A., "Fusion Welding of Aluminum Alloys," *British Welding Journal* 2 (9), 1954, 553 to 560.

24. McLachlan, N. W., *Complex Variable Theory and Transform Calculus with Technical Applications,* 2nd ed. Cambridge Eng. University Press 1953.

Appendix 1

In cases where the aspect ratio a = plate half width/thickness is of the order of unity, the effect of the vertical boundary planes parallel to the line of welding become important, and the representations (12) must be generalized to account for these effects. The appropriate formulas may be obtained using the method of images giving

$$u = \frac{1}{\tau^*} \sum_{n=-\infty}^{\infty} \sum_{m=-\infty}^{\infty} A_{nm}$$

$$A_{nm} \equiv \frac{\exp-\tau\{\xi+[\xi^2+(2n+\eta)^2+(2ma+\zeta)^2]^{1/2}\}}{[\xi^2+(2n+\eta)^2+(2ma+\xi)^2]^{1/2}},$$

for $\mu \to 0$. The corresponding formula for $\mu \to \infty$, is the same except with a factor $(-1)^n$ multiplying the terms in the double series.

Appendix 2

The solution for a finite conductivity backup bar can be obtained from the boundary value problem

$$\left(\frac{\partial}{\partial t} - \Delta\right) T_1 = \beta\delta(x-Vt)\delta(y)\delta(z),$$

$$0 \leq z \leq 1 \text{ (workpiece region)}$$

$$\left(\omega \frac{\partial}{\partial t} - \Delta\right) T_2 = 0,$$

$$z \geq 1 \text{ (backup bar region)}$$

$$T_1(x,y,1,t) = T_2(x,y,1,t)$$

$$\mu \frac{\partial T_1}{\partial z}(x,y,1,t) = \frac{\partial T_2}{\partial z}(x,y,1,t)$$

$$T_2(x,y,z,t) < \infty \text{ as } z \to \infty$$

$$T_1(x,y,z,0) = T_2(x,y,z,0) = 0$$

where the dimensionless temperature differences from the ambient temperature, T_∞, are expressed in units of $T_m - T_\infty$, the time is normalized with respect to ℓ^2/D_1, the quantity, $\omega \equiv D_1/D_2$, the D_i's are the thermal diffusivities of the workpiece and backup respctively, and the δ's are delta functions. Also, $\Delta \equiv \frac{\partial^2}{\partial x^2} + \frac{\partial^2}{\partial y^2} + \frac{\partial^2}{\partial z^2}$, and $\beta \equiv QD_1/k_1\ell^3(T_m - T_\infty)$. Using Green's functions and transform methods, the solution may be written in the form:

$$T_k = \int_0^t G_k(x-Vt', y, z, t-t')dt' \qquad (A2)$$

$$k = 1,2$$

$$G_1 = \frac{\theta}{4\pi^2 i}\int_0^\infty \sigma J_0(\sigma r)\,d\sigma \int_{Br} \tilde{f}\,dp \qquad (A3a)$$

$$\tilde{f} \equiv \frac{\mu\eta_1 \cosh\eta_1(1-z) + \eta_2 \sinh\eta_1(1-z)}{\mu\eta_1 \sinh\eta_1 + \eta_2 \cosh\eta_1} e^{pt} dp$$

$$G_2 = \frac{\theta\mu}{4\pi^2 i}\int_0^\infty \sigma J_0(\sigma r)\,d\sigma \int_{Br} \tilde{h}\,dp \qquad (A3b)$$

$$\tilde{h} \equiv \frac{e^{\eta_2(1-z)+pt} dp}{\mu\eta_1 \sinh\eta_1 + \eta_2 \cosh\eta_1}$$

where $\eta_1^2 \equiv p + \sigma^2$, $\eta_2 \equiv \omega p + \sigma^2$, and the Br's on the inner integrals in (A3) signify the appropriate Bromwich inversion contour in the p plane*, and J_0 signifies the Bessel function of zero order. Further reduction involves a detailed analysis of the residues and poles of the integrands and will not be discussed here. Instead, considerable simplification results when the physically realistic approximation (high conductivity backing) is used as a basis for the asymptotic expansions. The value of $T_1^{(1)}$ in the asymptotic expansion

$$T_1 = T_1^{(0)} + \mu T_1^{(1)} + \cdots \quad \text{as} \quad \mu \to 0$$

can be obtained as:

$$T_1^{(1)} = \frac{\sqrt{\omega}}{4\pi^2 3}\sum_0^\infty (-1)^n (n+1) \times \left\{ I(2(n+1)-z, y, t) + I(2(n+1)+z, y, t) \right\}$$

where

$$I(a,x,y,t) \equiv a^2 \int_0^t \frac{e^{-a^2/4\theta}}{\theta^{3/2}} d\theta \int_\theta^t \tilde{g}\,d\tau$$

$$\tilde{g} \equiv \frac{\exp-\{\omega[(x-V(t-\tau))^2+y^2]/4[\tau-(1-\omega)\theta]\}}{[\tau-(1-\omega)\theta]\sqrt{\tau-\theta}}$$

Similar methods can be used to obtain the solution for the effect of a large, but finite, perfectly conducting backing bar as an asymptotic expansion in terms of the previously introduced heat capacity parameter, ν tending to zero. A complete discussion of these solutions will be given in a future publication.

See Ref. 24 for example to obtain details on such integrations.